Molecular determinants of Ebola nucleocapsid stability from molecular dynamics simulations ()

Cite as: J. Chem. Phys. 153, 155102 (2020); https://doi.org/10.1063/5.0021491 Submitted: 10 July 2020 • Accepted: 18 September 2020 • Published Online: 20 October 2020

🗓 Chaoyi Xu, 🗓 Nidhi Katyal, 🗓 Tanya Nesterova, et al.

COLLECTIONS

Paper published as part of the special topic on Classical Molecular Dynamics (MD) Simulations: Codes, Algorithms, Force fields, and Applications



This paper was selected as Featured







ARTICLES YOU MAY BE INTERESTED IN

Scalable molecular dynamics on CPU and GPU architectures with NAMD The Journal of Chemical Physics 153, 044130 (2020); https://doi.org/10.1063/5.0014475

Use the force! Reduced variance estimators for densities, radial distribution functions, and local mobilities in molecular simulations

The Journal of Chemical Physics 153, 150902 (2020); https://doi.org/10.1063/5.0029113

MDBenchmark: A toolkit to optimize the performance of molecular dynamics simulations The Journal of Chemical Physics 153, 144105 (2020); https://doi.org/10.1063/5.0019045





Molecular determinants of Ebola nucleocapsid stability from molecular dynamics simulations •

Cite as: J. Chem. Phys. 153, 155102 (2020); doi: 10.1063/5.0021491 Submitted: 10 July 2020 · Accepted: 18 September 2020 ·

Published Online: 20 October 2020













AFFILIATIONS

Department of Chemistry and Biochemistry, University of Delaware, Newark, Delaware 19716, USA

Note: This paper is part of the JCP Special Topic on Classical Molecular Dynamics (MD) Simulations: Codes, Algorithms, Force Fields, and Applications.

^{a)}Author to whom correspondence should be addressed: jperilla@udel.edu

ABSTRACT

Ebola virus (EBOV) is a human pathogen with the ability to cause hemorrhagic fever and bleeding diathesis in hosts. The life cycle of EBOV depends on its nucleocapsid. The Ebola nucleocapsid consists of a helical assembly of nucleoproteins (NPs) encapsidating single-stranded viral RNA (ssRNA). Knowledge of the molecular determinants of Ebola nucleocapsid stability is essential for the development of therapeutics against EBOV. However, large degrees of freedom associated with the Ebola nucleocapsid helical assembly pose a computational challenge, thereby limiting the previous simulation studies to the level of monomers. In the present work, we have performed all atom molecular dynamics (MD) simulations of the helical assembly of EBOV nucleoproteins in the absence and presence of ssRNA. We found that ssRNA is essential for maintaining structural integrity of the nucleocapsid. Other molecular determinants observed to stabilize the nucleocapsid include NP-RNA and NP-NP interactions and ion distributions. Additionally, the structural and dynamical behavior of the nucleocapsid monomer depends on its position in the helical assembly. NP monomers present on the longitudinal edges of the helical tube are more exposed, flexible, and have weaker NP-NP interactions than those residing in the center. This work provides key structural features stabilizing the nucleocapsid that may serve as therapeutic targets.

© 2020 Author(s). All article content, except where otherwise noted, is licensed under a Creative Commons Attribution (CC BY) license (http://creativecommons.org/licenses/by/4.0/). https://doi.org/10.1063/5.0021491

I. INTRODUCTION

Ebola is an acute viral infection marked by hemorrhagic fever and bleeding diathesis, with the mortality rate ranging from 50% to nearly 90%. The aetiological agent of the disease is Ebola virus (EBOV). EBOV is an enveloped, negative sense single-stranded RNA (ssRNA) virus, which belongs to the Filoviridae family of the Mononegavirales order.² The Mononegavirales order includes several human pathogens such as rabies virus, respiratory syncytial virus, mumps virus, measles virus, and Marburg virus, which are characterized by their ssRNA genomes.3

The life cycle of EBOV is highly dependent on helical/tubular assemblies of one of the structural proteins in the virus called nucleoprotein (NP).4 The EBOV NP comprises an N-terminal tail, an N-terminal arm, a folded alpha helical NP core containing Nand C-terminal lobes, flanked by a disordered linker, and a Cterminal tail.^{5,6} NP monomers assemble in a helical arrangement

and encapsidate a single-stranded viral RNA genome (ssRNA) to form a complex called nucleocapsid. 6-9 Nucleocapsids protect the viral genome from recognition by cellular defense mechanisms and form a minimal functional unit for viral transcription and replication.⁴ NP oligomerization has been reported to either precede RNA clamping or to occur simultaneously. Nevertheless, both processes, namely, NP oligomerization and RNA clamping, are highly cooperative.6

The structural integrity of the EBOV rod-like helical nucleocapsid is essential for its biological function. 6,10 Similar rod-like nucleocapsids are present in other viruses including coronaviruses (e.g., SARS-CoV and SARS-CoV-2),¹¹ Marburg virus,¹² Rabies virus, 13 and tobacco mosaic virus. 14 For some of these viruses, helical assemblies of NPs without RNA are stable, 15 while for others, RNA binding is required for nucleocapsid stability.¹⁶ For EBOV, although the interaction site of RNA with NP is known (PDB: 5Z9W⁶), whether RNA regulates cohesion of the assembled nucleocapsid is still not clear. Knowledge of the molecular determinants of EBOV nucleocapsid stability, such as packaging of genetic material, electrostatic potential of the system, and arrangement of residues in the helical assembly, ^{15,17–21} is critical for therapeutic intervention. Such insights are inaccessible via traditional experimental means but are readily obtainable from computer simulations.

Molecular dynamics simulations (MD) of large biomolecules have been performed for systems of varying sizes and complexities. 15,22-28 However, simulating large assemblies of nucleocapsids at an atomic resolution still present a computational challenge. With the exceptions of HIV-1 and satellite tobacco mosaic virus, 17,29 MD simulations of large viral assemblies of nucleocapsids performed thus far have been carried out at the level of monomers. 28,30-35 Structural and dynamical knowledge of these assemblies is essential to reveal molecular determinants for the integrity of the nucleocapsids. Here, to the best of our knowledge, for the first time, we present MD simulations of the EBOV nucleocapsid helical assembly and provide insights into the physicochemical properties regulating its stability.

II. METHODS

Preparation of EBOV nucleocapsid systems for MD simulations. Simulations of nucleocapsids require careful treatment of the electrostatic interactions between protein, RNA, and solvent. ^{17,25} The initial structures and the series of steps taken to prepare for MD simulations of EBOV NP are shown in Figs. 1(a)-1(c) (Multimedia view). First, the protonation states of titratable residues in the NP were determined using PROPKA³⁶ at a physiological pH of 7.0. Second, starting from a single NP-RNA monomer [Fig. 1(a) (Multimedia view), PDB: 5Z9W⁶], a helical assembly of an EBOV nucleoprotein was built by rigid-body fitting 90 NP monomers into the corresponding 3.6 Å resolution cryo-EM density (EMID: 6903⁶) using Chimera.³⁷ The ssRNA present in the nucleocapsid was built by combining the RNA fragments bound to each NP monomers [PDB: 5Z9W, Fig. 1(b) (Multimedia view) into a single chain [Figs. S1(a)– S1(c)]. The ssRNA is a chain of Uracil nucleotides, the same as in the EBOV nucleocapsid monomer structure (PDB: 5Z9W⁶). NP interaction with RNA is reported to be sequence-independent. The quality of fitting of the nucleocapsid into the experimental density was determined using the Fourier shell correlation (FSC) and the golden standard cutoff, as shown in Figs. S2(a)-S2(c). Subsequently, Na⁺ and Cl⁻ were added in close proximity to the nucleocapsid using CIONIZE in Visual Molecular Dynamics (VMD),²⁵ based on the local electrostatic potential. Solvation of the entire system was performed using the TIP3P water model,³⁹ and the total bulk concentration of NaCl was set to 150 mM, resulting in a simulation setup containing 4.8M atoms [Fig. 1(d) (Multimedia view)]. A control system without the ssRNA was built with the same protocol [Fig. 1(c) (Multimedia view)]. Both systems, namely, the nucleocapsid and the control system without the ssRNA, were then minimized for 10000 steps using a conjugate gradient⁴⁰ and line search algorithm,41 with all backbone atoms of the nucleoprotein and ssRNA fixed, followed by equilibration using molecular dynamics flexible fitting (MDFF)⁴² into the cryo-EM density (EMD-6903). Thereafter, the systems were heated from 50 K to 310 K in 20 K increments for 1 ns while constraining the backbone atoms. Subsequently, the systems were equilibrated for 10 ns.

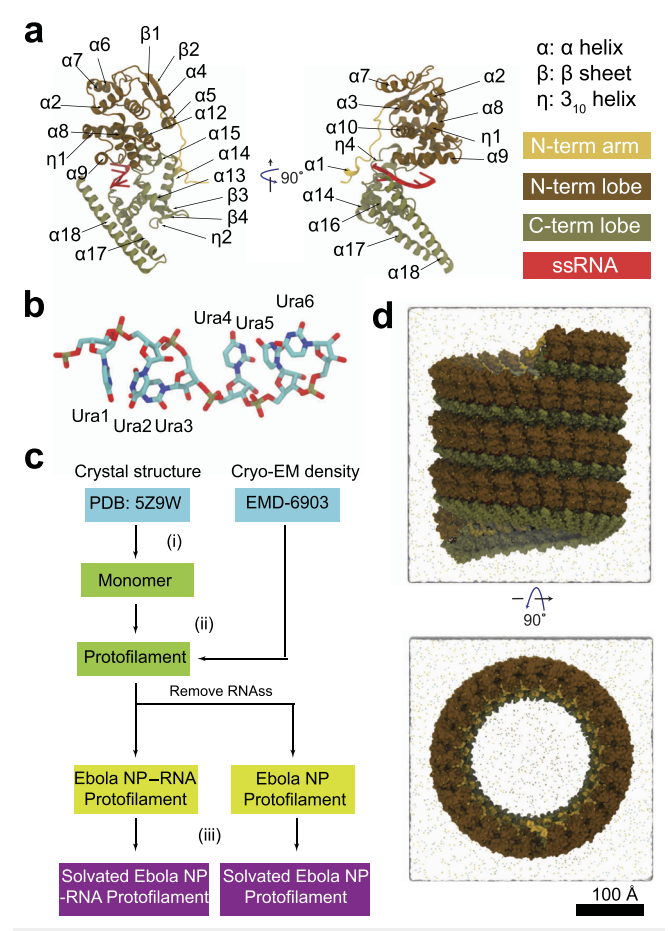


FIG. 1. Preparation of EBOV nucleocapsid systems for atomistic molecular dynamics simulations. (a) Structure of the EBOV nucleocapsid monomer (PDB: 5Z9W⁶), containing three nucleoprotein structural domains: the N-terminal arm (yellow), N-terminal lobe (brown), and C-terminal lobe (dark green), and a bound RNA segment (red). (b) Atomic representation of RNA nucleotides in an EBOV nucleocapsid monomer. (c) Flowchart to prepare the EBOV nucleocapsid systems for molecular dynamics simulations: (i) First, the protonation states of titratable residues in the nucleocapsid monomer derived from the cryo-EM structures was computed. (ii) Subsequently, EBOV nucleocapsid complexes were built by rigid-body fitting 90 nucleocapsid monomers into the cryo-EM density using Chimera. (iii) Finally, the complexes were solvated with TIP3P water molecules and neutralized. NaCl concentration was kept to 150 mM. (d) Representation of the constructed EBOV nucleocapsid system. The sodium and chloride ions are shown as yellow and cyan spheres. Multimedia view: https://doi.org/10.1063/5.0021491.1

During equilibration, the cryo-EM density (EMD-6903) was applied as a restraint with a coupling factor of 0.1 in MDFF to maintain the conformation of the NP complex prior to production runs (Fig. S3).

MD simulations of EBOV nucleocapsid. The EBOV nucleocapsids without and with RNA were simulated for 100 ns at 310 K and 1 atm using the stochastic rescaling thermostat⁴³ and the Nosé-Hoover Langevin-piston pressure control, as implemented in NAMD 2.14.⁴⁴ All bonds to hydrogen were constrained with the SHAKE and SETTLE algorithm for the solute and solvent, respectively. Long range electrostatic force calculations used the

particle mesh Ewald method, with a 1.2 nm cutoff. The r-RESPA integrator and an integration time step of 2 fs were utilized, with the nonbonded interactions evaluated every 2 fs and electrostatics updated every 4 fs. CHARMM36m protein⁴⁵ and CHARMM TIP3P water³⁹ force fields were employed in MD simulations.

Analysis of MD Simulation. All post-simulation analyses were performed on the trajectories, discarding the initial 20 ns. Ion occupancies of sodium and chloride ions were computed using the VolMap plugin in VMD.³⁸ VMD was also used to compute contacts between NP-RNA and NP-NP residues through a TCL script in which residue contacts were defined as closest inter-residue distances less than 3.4 Å. Principal component analysis (PCA) of the EBOV nucleocapsid was performed using a method described in a previously published paper. 46 First, the equilibrated MD trajectory of the Cα atoms of the Ebola nucleoprotein was centered and aligned. Then, PCA was performed for Cα atoms on 8000 snapshots each at 10 ps intervals. Using an in-house script, 46 8000 modes were calculated. The cumulative contribution to variance W^k for the first k PCs was calculated with the following equation: $W^k = \frac{\sum_{i=1}^k \lambda_i}{\sum_{k=0}^{8000} \lambda_i}$, where λ_i is the eigenvalue of the *i*th PC. The PCA figures were produced using VMD with NMWiz.4

Electrostatic potential calculations. An electrostatic potential map of the EBOV nucleocapsid was generated by numerically solving the nonlinear Poisson–Boltzmann equation using the Adaptive Poisson–Boltzmann Solver (APBS) software. To prepare the input structure for APBS, PDB2PQR⁴⁹ was used with the CHARMM allatom force field, and the protonation states of residues corresponded to a pH value of 7. The calculations were performed in parallel using the multigrid approach at a temperature of 310 K. An ionic strength of 150 mM was used for monovalent ions. Positive and negative ions were assigned radii of 0.95 Å and 1.81 Å, corresponding to sodium and chloride, respectively. The external dielectric constant of the solvent was kept as 78.54, and the solute dielectric constant was set to 2. A cubic grid of 1025 grid points per side was used, and the atomic partial charges to grid points were mapped using cubic B-spline discretization.

III. RESULTS

To characterize the molecular determinants of stability, we have built helical assemblies of NPs, with and without the bound RNA strand, and have performed all-atom MD simulations on these two

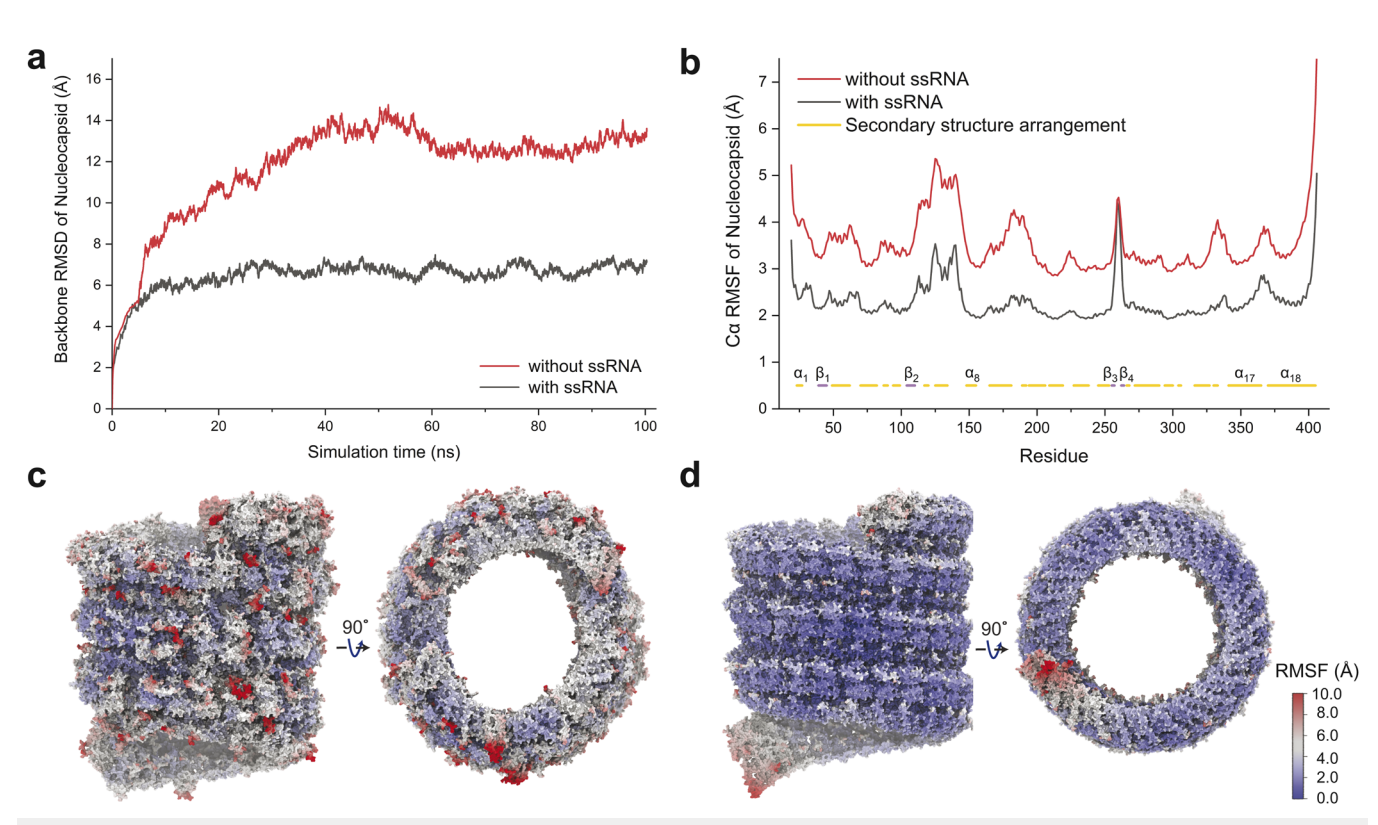


FIG. 2. Structural integrity of the EBOV nucleocapsid complexes. (a) Root-mean-squared deviations (RMSDs) of the backbone atoms of the Ebola nucleoprotein assembly with and without ssRNA, as a function of simulation time. (b) Averaged root mean square fluctuations (RMSFs) of NP monomers in EBOV NP and EBOV NP-RNA. The secondary structure assignments of a nucleoprotein monomer are shown at the bottom of the plot. The regions forming helices are represented as yellow lines, and those forming beta sheets are shown by purple lines. (c) Molecular surface representation of EBOV NP. (d) Molecular surface representation of EBOV NP-RNA. The color bar on the right shows the RMSF values of the NPs in (c) and (d). Multimedia view: https://doi.org/10.1063/5.0021491.2

systems for 100 ns. Throughout the manuscript, we refer to the former system as EBOV NP-RNA and the latter as EBOV NP.

The structural integrity of the constructed EBOV NP and EBOV NP-RNA was first assessed by calculating the root-meansquared deviation (RMSD) with respect to the initial structure over the course of the simulation [Fig. 2(a) (Multimedia view)]. RMSD traces of the backbone of the entire NP assembly in the absence of RNA show an overall change of around 14 Å from the initial structure, before reaching the plateau. Conversely, the corresponding deviations in the presence of ssRNA plateau at a far smaller value of 6 Å after 20 ns of simulation. Thus, the EBOV NP assembly shows less structural deviations when RNA binds to it.

The flexibility of the assembled nucleocapsid was evaluated by computing root mean square fluctuations (RMSFs) of alpha carbon atoms of the nucleoprotein in EBOV NP and EBOV NP-RNA, as shown in Fig. 2(b) (Multimedia view). The loop regions at the terminals and between the β -strands 3 and 4 are highly mobile. Additionally, residues between β -strand 2 and α -helix 8 in the Nterminal lobe also display high flexibility. Nucleoprotein residues in both systems follow a similar trend in the RMSF values. However, for EBOV NP, the magnitude of fluctuations is higher. Furthermore, the regions with high RMSF values (>6 Å) distribute throughout the assembly [Fig. 2(c) (Multimedia view)]. On the other hand, in EBOV NP-RNA, the regions with high RMSF values are located at the longitudinal edges of the assembly [Fig. 2(d) (Multimedia view)]. Overall, the binding of ssRNA decreases the flexibility of nucleoprotein residues in the EBOV nucleocapsid, thereby stabilizing the entire assembly.

The significance of ssRNA in maintaining structural integrity of the helical nucleocapsid was determined by comparing simulations of the helical EBOV NPs in the absence and presence of ssRNA. The structures of EBOV NP and EBOV NP-RNA after MD simulations are shown in Figs. 2(c) and 2(d) (Multimedia view). Without RNA, the EBOV nucleocapsid maintains its tubular morphology, but the packing of NP monomers in the assembly become disordered [Fig. 2(c) (Multimedia view)], and thus, the helical symmetry of the NP assembly is nearly demolished. This finding is consistent with the large structural deviation observed in EBOV NP [Fig. 2(a) (Multimedia view)]. On the other hand, the helical arrangement in the EBOV NP-RNA assembly is preserved in MD simulation [Fig. 2(d) (Multimedia view)]. Together, these results indicate that RNA binding stabilizes the helical arrangement and structure of the EBOV nucleocapsid.

To identify important NP-RNA interactions, the occupancies of NP residues involved in interactions with the ssRNA during the EBOV NP-RNA MD simulation were evaluated and are listed in Table S1. The RNA segment in the NP monomer makes contacts with residues of NP in its own binding site as well as neighboring NP residues, outside of its binding site, at an occupancy greater than 90% [Fig. S5(a), Table S1]. NP residues involved in the interactions with ssRNA are consistent with those reported in the literature.^{6,50} A majority of these reported

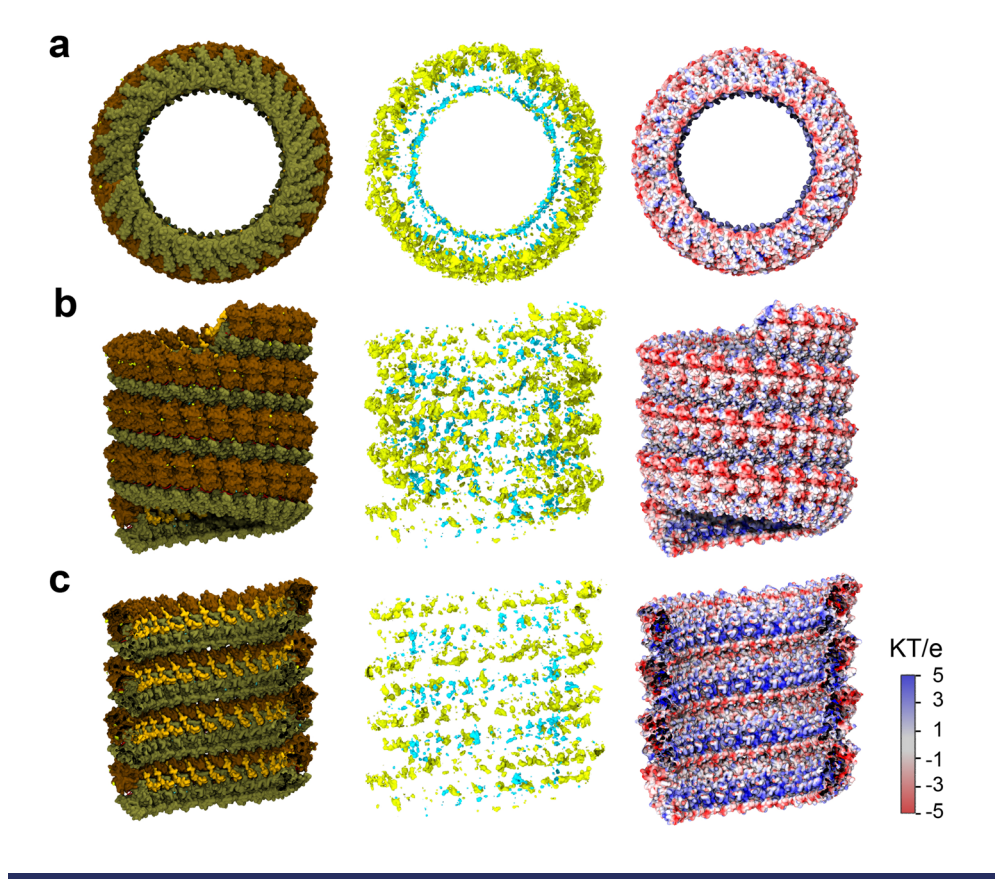


FIG. 3. Sodium and chloride ions neutralize the highly charged EBOV nucleocapsid. (a) Sodium (yellow) and chloride (cyan) ion occupancies. The ion occupancies were calculated by averaging over the last 80 ns of EBOV NP-RNA simulation. The isovalues of the occupancies are 0.01. (b) The electrostatic potential map of the entire EBOV nucleocapsid, calculated using Adaptive Poisson-Boltzmann Solver (APBS). The ion occupancies and the electrostatic potential map are represented from three viewpoints, top view, a side view, and a cross section of the sideview, from top to bottom.

interactions have an occupancy greater than 60% in the present simulation (Table S1). Notably, we have also observed several additional NP residues that binds with RNA that were not reported in the literature, ^{6,51} for example, Val163 (99.6% occupancy) and Gly311 (91.9% occupancy). Overall, the ssRNA is found to have considerable interactions with the EBOV nucleocapsid, and these are well-maintained during the simulation and contribute to the stability of the EBOV nucleocapsid.

Besides NP-RNA interactions, the residue contacts between neighboring NP monomers also play a vital role in EBOV NP oligomerization and the nucleocapsid structural stability and integrity. 6,50-52 Based on the NP monomers that they connect, the NP-NP interfaces can be grouped into intra-strand and inter-strand interfaces, as shown in Figs. S4(a)-S2(f). The intra-strand interfaces permit lateral interactions between NP subunits (NPn and $\mathrm{NP}^{\mathrm{n+1}}$). Three major intra-strand interfaces, labeled interface 1, 2 and 3, respectively, are present [Figs. S4(a)-S4(d) and S5(b)-S2(d)]. Residues that form contacts at these three interfaces along with their percentage occupancies in the MD simulations are shown in Table S2. In EBOV NP, no NP-NP residue contact formed at any three intra-stand interfaces has an occupancy greater than 70%. Inversely, many intra-strand interactions in EBOV NP-RNA have occupancies greater than 90%, pointing to the role of RNA in stabilizing nucleocapsids. Many NP-NP intra-strand interactions observed in our simulations are consistent with those reported in the previous cryo-EM structure.^{6,50}

The inter-strand interfaces, on the other hand, are formed between neighboring NP monomers in the axial direction, i.e., parallel to the tubular axis of the nucleocapsid. Two inter-strand interfaces, Interface 4 (between NPⁿ and NPⁿ⁻²⁴) and Interface 5 (between NPⁿ and NPⁿ⁻²⁵) are present in the assembly, as shown in Figs. S4(e), S4(f), S5(e), and S5(f). The NP-NP contacts at the interstrand interfaces and their occupancies are listed in Table S3. The contacts between residues in all inter-stand interfaces were found to have occupancy values less than 40% in the EBOV NP system. However, in EBOV NP-RNA, the corresponding occupancies are significantly higher. This observation is similar to the intra-strand NP-NP interaction described above. Three residue contacts are found with an occupancy greater than 60%, namely, Lys110-Glu345, Asp112-Lys399, and Glu107-Lys382. Taken together, these results underline the critical role of the NP-NP interactions at the intraand inter-strand interfaces in maintaining the stability of the EBOV nucleoprotein tubular assembly.

Ions play a pertinent role in stabilizing viral nucleocapsids. ^{15,53} In EBOV NP-RNA, the ssRNA holds a negative charge of -539e, while the 90 nucleoprotein monomers contribute a net positive charge of +360e. The distribution of sodium and chloride ions in the system was analyzed by identifying regions of high ion occupancies in the simulation, as shown in Fig. 3(a). Sodium ions prefer to reside around the ssRNA binding pocket [Fig. 3(b)] and pockets in the NP monomers and between NP intra-strand interfaces, formed by acidic residues [Fig. 3(b). Chloride ions, on the other hand, arrange themselves between NP intra-strand interfaces with nearby loci formed by basic amino acids [Fig. 3(b). Overall, positively charged sodium ions are distributed in the outer circumference, and chloride ions are mostly located in the inner circumference of the nucleoprotein helical assembly [Figs. 3(a) and 3(b)]. These ions neutralize the EBOV nucleocapsid and further contribute to its stability.

After MD simulation, although the helical assembly of the EBOV nucleocapsid was mostly sustained, the nucleoproteins at two longitudinal ends were partially unwound [Fig. 4(a)]. To monitor the unwinding process, the inter-strand distances between NPⁿ and NPⁿ⁻²⁴ were calculated as shown in Fig. 4(b). The corresponding distances for residues located at the two edges of the nucleocapsid assembly were found to increase considerably during the simulation. However, the inter-strand distances for residues located anywhere else in the rest of the strand were almost constant after 10 ns. On

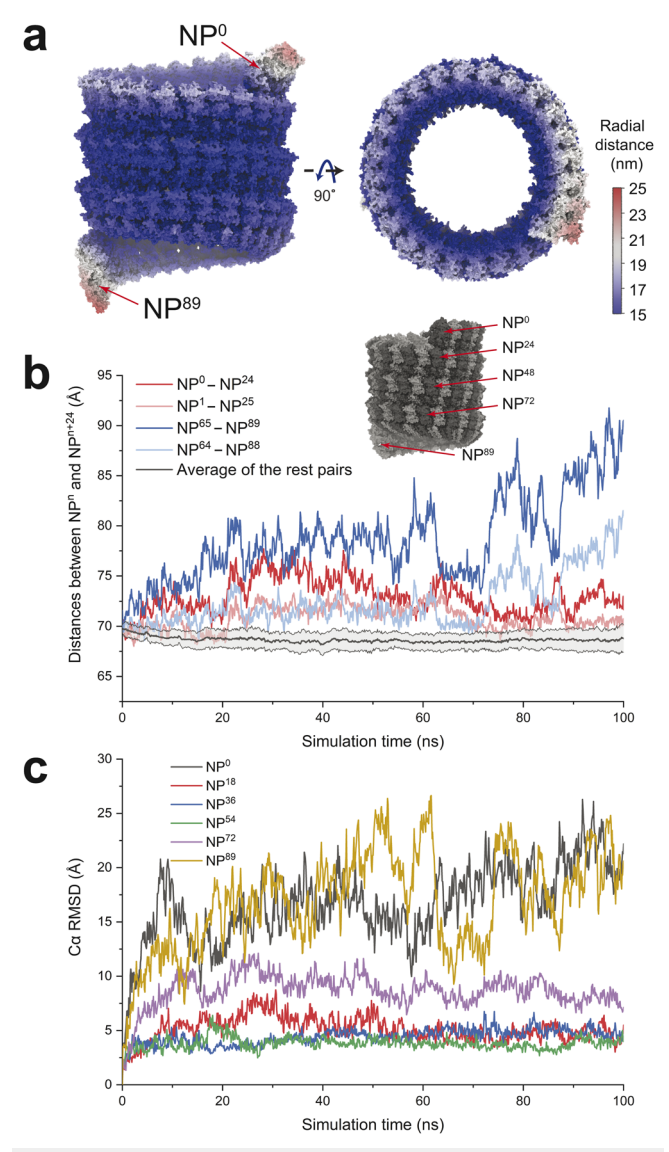


FIG. 4. Structural instability of the edges in EBOV NP–RNA. (a) The EBOV nucleocapsid after 100 ns of MD simulation. It is colored by the radial distance from its center of mass. (b) NPⁿ–NPⁿ⁺²⁴ distances along the tubular axis of nucleocapsid as a function of simulation time, n = 0, 1, 64, and 65. The average and standard deviation of the rest NP–NP pairs are shown in black and gray traces, respectively. (c) Time evolution of Cα atom RMSDs of NP monomers present on the edges (NP⁰, NP¹⁸, NP⁷², and NP⁸⁹) and center (NP³⁶ and NP⁵⁴) of the nucleocapsid.

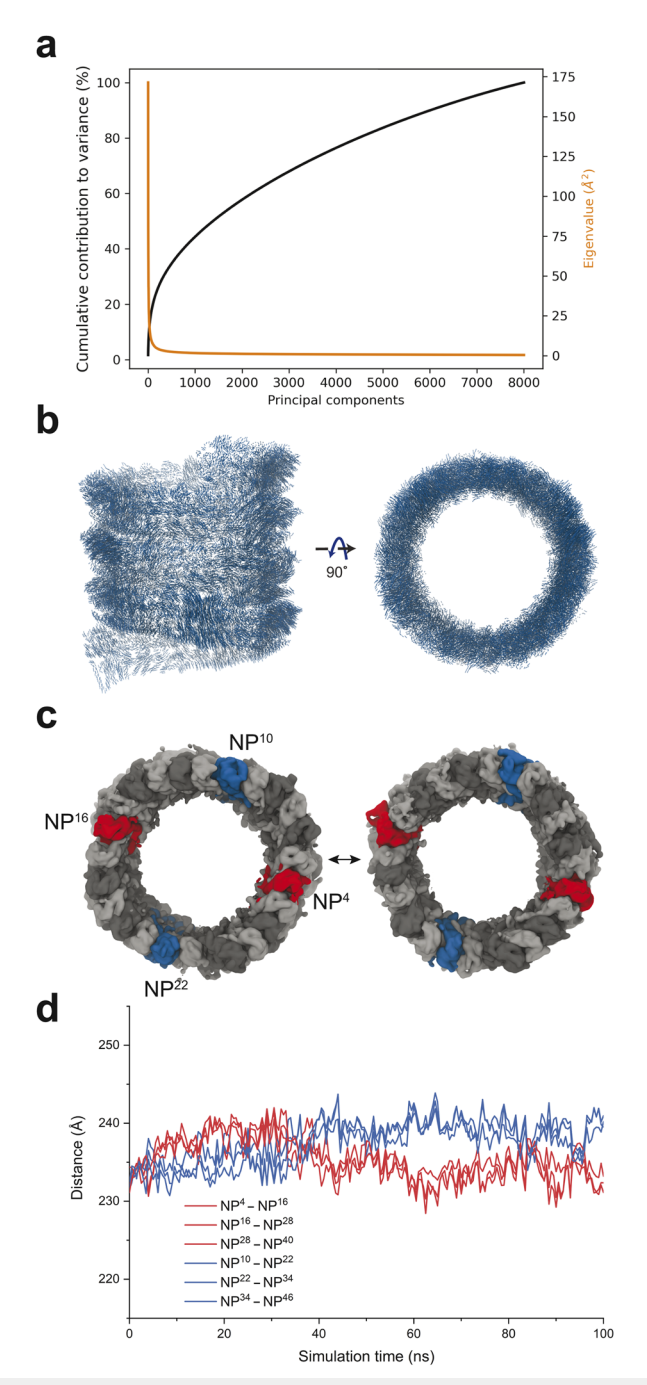


FIG. 5. Principal component analysis (PCA) of the Ebola NP–RNA. (a) Cumulative contributions to variance and the eigenvalues of the first 8000 PCs. The PCs were calculated via a protocol described in our previous work. ⁴⁶ (b) Porcupine plot showing PCA dominating motions for the EBOV nucleocapsid averaged over the first 100 eigenvectors. The arrows indicate the direction of the eigenvector, and their lengths represent the magnitude of the corresponding value. (c) Two extreme conformations of the EBOV nucleocapsid sampled during the simulation along the average of the first 100 eigenvectors. (d) Distances between the center of masses of NP monomers on opposing sides of the helical nucleocapsid as a function of simulation time. Multimedia view: https://doi.org/10.1063/5.0021491.3

similar lines, the nucleocapsid monomers at the two edges of the nucleocapsid assembly showed large structural deviations [Fig. 4(c)] compared to the monomers located in the center of the assembly. These results suggest a positional dependence of the structural integrity in the EBOV nucleocapsid.

Principal Component Analysis (PCA)^{54–56} has been employed to identify motions relevant to the biological assembly of the Ebola nucleocapsid. The first 8000 PCs of the Ebola NP-RNA were computed. Their eigenvalues and the cumulative contribution to variance are shown in Fig. 5(a) (Multimedia view). The first 1000 PCs account for about 50% of total variance. The motions obtained by averaging the first 100 PCs and the first three PCs of EBOV NP-RNA are illustrated in Fig. 5(b) (Multimedia view) and Fig. S6, respectively. These motions contain not only local rearrangements of the nucleoprotein monomers in the assembly but also many global motions of the EBOV nucleocapsid. For example, one such global motion observed at one edge of the EBOV NP-RNA is depicted in Fig. 5(c) (Multimedia view). It corresponds to an anti-correlation in the motions of EBOV nucleocapsid, which is represented by the changes in the NP-NP distances observed during the simulation [Fig. 5(d) (Multimedia view)]. When the NP⁴-NP¹⁶ distance increases, the NP¹⁰-NP²² distance decreases, and vice versa. Other motions identified by the PCA analysis are shown in Fig. S6. These global and local slow motions found in the EBOV nucleocapsid from PCA suggests the dynamic nature of the EBOV nucleocapsid and could be important to its biological function, for example, binding with other viral proteins.

IV. DISCUSSION

The life cycle of EBOV depends on its nucleocapsid, which assembles into a helical arrangement and encapsidates the viral genomes. Knowledge of the key determinants stabilizing this helical assembly is crucial in developing antiviral therapeutics. Herein, we have modeled helical assemblies of EBOV nucleoprotein with and without ssRNA, using the available cryo-EM density map, and performed molecular dynamics simulations to identify the molecular determinants that control the stability of the Ebola virus nucleocapsid.

The stability of the nucleocapsid depends on its structural and dynamical properties. The structure of the EBOV nucleocapsid assembly is regulated by interactions between all of its possible components, viz., NP–NP and NP–RNA, as well as interactions of these components with the surrounding solution. On the other hand, global and local fluctuations in the nucleocapsid govern its dynamical behaviors. Here, each of these determinants is analyzed in detail at atomic resolution.

The prominent NP–NP and NP–RNA interactions extracted from our simulation includes few other interactions in addition to those observed previously. In addition, some interactions were reported in the literature but were found to have low occupancy (Tables S1–S3). Overall, the occupancies of NP–NP and NP–RNA interactions in EBOV nucleocapsid simulation are considerably large, contributing to its stability. Importantly, we found that residues in nucleotide free simulations are highly mobile, resulting in remarkably weaker NP–NP interactions, specifically in the lateral direction. Thus, ssRNA encapsidation results in stabilization of

the EBOV nucleocapsid and is essential for maintaining structural integrity of its helical assembly.

Ions influence the electrostatic potential of the EBOV nucleocapsid and contribute to its stability. ^{15,53} Ions surrounding the assembled nucleocapsid were observed to have high occupancies in regions of high electrostatic potential. Although the exact significance of these interaction sites is not known, they are speculated to constitute protein–protein interaction interfaces of viral accessory proteins and yet undiscovered cellular factors.

Analysis of the local fluctuations reveals that the residues in the helical assembly of the EBOV nucleocapsid display dynamical behavior depending on their position in the helix. Longitudinal edges were found to be more flexible compared to the center of the EBOV helical nucleocapsid. These edges unwind during the course of simulation. The dissimilarity in stability and dynamicity between the edges and central part of the nucleocapsid could stem from differences in the surrounding chemical environment, particularly the absence of the NP–NP interactions at the edges. Furthermore, we have performed PCA to identify the slow motions bringing about the conformational changes in the nucleocapsid assembly. Global motions of the whole assembly and local rearrangements of the NP monomers were both observed. These motions could be important to the biological functions of the nucleocapsid during the EBOV infection and replication.

Taken together, the present manuscript sheds light onto the roles of ions, NP-NP interactions, and NP-RNA interactions in maintaining the structural integrity of the EBOV nucleocapsid. We demonstrated that ssRNA is essential for the assembly of EBOV NPs. Molecular determinants of the stability of the nucleocapsid determined from the present work can be exploited to modulate EBOV nucleocapsid functionalities. Key structural features stabilizing the nucleocapsid may serve as therapeutic targets. In addition, we present a systematic way of modeling and analyzing the structural and dynamical properties of the helical assembly of the nucleoprotein. We anticipate that the methodological development presented herein will guide others in the simulation of similar helical assemblies.

SUPPLEMENTARY MATERIAL

A total of six supplementary figures and three tables are included as the supplementary material to support the findings in the present manuscript.

AUTHORS' CONTRIBUTIONS

C. Xu and N. Katyal contributed equally to this work.

ACKNOWLEDGMENTS

This work was supported by the National Science Foundation (Award No. MCB-2027096), funded, in part, by the Delaware Established Program to Stimulate Competitive Research (EPSCoR). The authors acknowledge funding from the US National Institutes of Health (Award Nos. P50AI1504817 and P20GM104316). This research is part of the Frontera computing project at the Texas Advanced Computing Center. Frontera is made possible by the NSF

(Award No. OAC-1818253). This work used the Extreme Science and Engineering Discovery Environment, which is supported by the National Science Foundation (Grant No. ACI-1548562). This work used XSEDE Bridges and Stampede2 at the Pittsburgh Super Computing Center and Texas Advanced Computing Center, respectively, through Allocation No. MCB170096. T.N. was supported by the University of Delaware's Summer Scholars and NSF's XSEDE EMPOWER.

DATA AVAILABILITY

The data that support the findings of this study are available from the corresponding author upon reasonable request.

REFERENCES

- ¹L. Baseler, D. S. Chertow, K. M. Johnson, H. Feldmann, and D. M. Morens, "The pathogenesis of Ebola virus disease," Annu. Rev. Pathol.: Mech. Dis. 12, 387–418 (2017).
- ²O. Dolnik, L. Kolesnikova, and S. Becker, "Filoviruses: Interactions with the host cell," Cell. Mol. Life Sci. **65**, 756–776 (2008).
- ³M. Luo, T. J. Green, X. Zhang, J. Tsao *et al.*, "Structural comparisons of the nucleoprotein from three negative strand RNA virus families," Virol. J. 4, 72 (2007).
- ⁴W. Wan, L. Kolesnikova, M. Clarke, A. Koehler, T. Noda, S. Becker, and J. A. Briggs, "Structure and assembly of the Ebola virus nucleocapsid," Nature 551(7680), 394–397 (2017).
- ⁵Z. Su, C. Wu, L. Shi, P. Luthra *et al.*, "Electron cryo-microscopy structure of Ebola virus nucleoprotein reveals a mechanism for nucleocapsid-like assembly," Cell 172, 966–978 (2018).
- ⁶Y. Sugita, H. Matsunami, Y. Kawaoka, T. Noda *et al.*, "Cryo-EM structure of the Ebola virus nucleoprotein–RNA complex at 3.6 Å resolution," Nature **563**, 137–140 (2018).
- ⁷P. Aleksandrowicz, A. Marzi, N. Biedenkopf, N. Beimforde *et al.*, "Ebola virus enters host cells by macropinocytosis and clathrin-mediated endocytosis," J. Infect. Dis. **204**, S957–S967 (2011).
- M. F. Hagan, "Modeling viral capsid assembly," Adv. Chem. Phys. 155, 1 (2014).
 J. D. Perlmutter, C. Qiao, and M. F. Hagan, "Viral genome structures are optimal for capsid assembly," eLife 2, e00632 (2013).
- ¹⁰T. Hoenen, A. Groseth, and H. Feldmann, "Therapeutic strategies to target the Ebola virus life cycle," Nat. Rev. Microbiol. 17, 593–606 (2019).
- ¹¹C. Y. Chen, C. K. Chang, Y. W. Chang, S. C. Sue *et al.*, "Structure of the SARS coronavirus nucleocapsid protein RNA-binding dimerization domain suggests a mechanism for helical packaging of viral RNA," J. Mol. Biol. 368, 1075–1086 (2007).
- ¹²T. A. M. Bharat, J. D. Riches, L. Kolesnikova, S. Welsch *et al.*, "Cryo-electron tomography of Marburg virus particles and their morphogenesis within infected cells," PLoS Biol. 9, e1001196 (2011).
- ¹³P. Guichard, T. Krell, M. Chevalier, C. Vaysse *et al.*, "Three dimensional morphology of rabies virus studied by cryo-electron tomography," J. Struct. Biol. **176**, 32–40 (2011).
- 14 D. K. Clare and E. V. Orlova, "4.6 Å cryo-EM reconstruction of tobacco mosaic virus from images recorded at 300 keV on a 4k \times 4k CCD camera," J. Struct. Biol. 171, 303–308 (2010).
- ¹⁵E. Tarasova, V. Farafonov, R. Khayat, N. Okimoto *et al.*, "All-atom molecular dynamics simulations of entire virus capsid reveal the role of ion distribution in capsid's stability," J. Phys. Chem. Lett. **8**, 779–784 (2017).
- ¹⁶S.-W. Wang, K. Noonan, and A. Aldovini, "Nucleocapsid-RNA interactions are essential to structural stability but not to assembly of retroviruses," J. Virol. 78, 716–723 (2004).
- ¹⁷P. L. Freddolino, A. S. Arkhipov, S. B. Larson, A. McPherson *et al.*, "Molecular dynamics simulations of the complete satellite tobacco mosaic virus," Structure 14, 437–449 (2006).

- ¹⁸Y. Wang, X. Wu, Y. Wang, B. Li *et al.*, "Low stability of nucleocapsid protein in SARS virus," Biochemistry **43**, 11103–11108 (2004).
- 19 C.-Y. Huang, Y.-L. Hsu, W.-L. Chiang, and M.-H. Hou, "Elucidation of the stability and functional regions of the human coronavirus OC43 nucleocapsid protein," Protein Sci. 18, 2209–2218 (2009).
 20 E. N. Prokudina, N. P. Semenova, and V. M. Chumakov, "Stability of intracel-
- ²⁰E. N. Prokudina, N. P. Semenova, and V. M. Chumakov, "Stability of intracellular influenza virus nucleocapsid protein oligomers," Arch. Virol. 150, 833–839 (2005).
- ²¹ J.-L. Darlix, J. Godet, R. Ivanyi-Nagy, P. Fossé *et al.*, "Flexible nature and specific functions of the HIV-1 nucleocapsid protein," J. Mol. Biol. **410**, 565–581 (2011).
- ²²Y. Zhao, B. L. Kormos, D. L. Beveridge, and A. M. Baranger, "Molecular dynamics simulation studies of a protein–RNA complex with a selectively modified binding interface," Biopolymers **81**, 256–269 (2006).
- ²³C. M. Reyes and P. A. Kollman, "Structure and thermodynamics of RNA-protein binding: Using molecular dynamics and free energy analyses to calculate the free energies of binding and conformational change," J. Mol. Biol. 297, 1145–1158 (2000).
- ²⁴J. K. Marzinek, R. G. Huber, and P. J. Bond, "Multiscale modelling and simulation of viruses," Curr. Opin. Struct. Biol. 61, 146–152 (2020).
- ²⁵J. A. Hadden and J. R. Perilla, "Molecular dynamics simulations of protein–drug complexes: A computational protocol for investigating the interactions of small-molecule therapeutics with biological targets and biosensors," in *Computational Drug Discovery and Design* (Springer, 2018), pp. 245–270.
- ²⁶ J. A. Hadden and J. R. Perilla, "All-atom virus simulations," Curr. Opin. Virol. 31, 82–91 (2018).
- ²⁷T. Reddy and M. S. P. Sansom, "Computational virology: From the inside out," Biochim. Biophys. Acta, Biomembr. **1858**, 1610–1618 (2016).
- ²⁸J. G. Pattis and E. R. May, "Markov state model of Lassa virus nucleoprotein reveals large structural changes during the trimer to monomer transition," Structure 28, 548–554.e3 (2020).
- ²⁹J. R. Perilla, B. C. Goh, C. K. Cassidy, B. Liu *et al.*, "Molecular dynamics simulations of large macromolecular complexes," Curr. Opin. Struct. Biol. 31, 64–74 (2015), part of Special Issue: Theory and Simulation/Macromolecular Machines and Assemblies.
- ³⁰ M. A. Olson, "Disorder-order transitions in conformational selection of a peptide by Ebola virus nucleoprotein," ACS Omega 5, 5691–5697 (2020).
- ³¹L. Li, D. Li, H. Chen, and J.-G. Han, "Studies on the binding modes of Lassa nucleoprotein complexed with m7GpppG and dTTP by molecular dynamic simulations and free energy calculations," J. Biomol. Struct. Dyn. **31**, 299–315 (2013).
- ³²B. Tarus, C. Chevalier, C.-A. Richard, B. Delmas *et al.*, "Molecular dynamics studies of the nucleoprotein of influenza A virus: Role of the protein flexibility in RNA binding," PLoS One 7, e30038 (2012).
- ³³R. N. Lima, M. Faheem, J. A. R. G. Barbosa *et al.*, "Homology modeling and molecular dynamics provide structural insights into tospovirus nucleoprotein," BMC Bioinf. 17, 489 (2016).
- ³⁴J. G. Pattis and E. R. May, "Influence of RNA binding on the structure and dynamics of the Lassa virus nucleoprotein," Biophys. J. **110**, 1246–1254 (2016).
- ³⁵Y. Zhang, H. Chen, and J.-G. Han, "Insight into the binding modes of Lassa nucleoprotein complexed with ssRNA by molecular dynamic simulations and free energy calculations," J. Biomol. Struct. Dyn. 33, 946–960 (2015).
- ³⁶M. H. M. Olsson, C. R. Søndergaard, M. Rostkowski, and J. H. Jensen, "PROPKA3: Consistent treatment of internal and surface residues in empirical pKa predictions," J. Chem. Theory Comput. 7, 525–537 (2011).
- ³⁷E. F. Pettersen, T. D. Goddard, C. C. Huang, G. S. Couch *et al.*, "UCSF chimera—A visualization system for exploratory research and analysis," J. Comput. Chem. **25**, 1605–1612 (2004).

- ³⁸W. Humphrey, A. Dalke, K. Schulten *et al.*, "VMD: Visual molecular dynamics," J. Mol. Graphics **14**, 33–38 (1996).
- ³⁹ W. L. Jorgensen, J. Chandrasekhar, J. D. Madura, R. W. Impey, and M. L. Klein, "Comparison of simple potential functions for simulating liquid water," J. Chem. Phys. **79**, 926–935 (1983).
- ⁴⁰R. Fletcher and C. M. Reeves, "Function minimization by conjugate gradients," Comput. J. 7, 149–154 (1964).
- ⁴¹W. Sun and Y.-X. Yuan, Optimization Theory and Methods: Nonlinear Programming (Springer Science & Business Media, 2006), Vol. 1.
- ⁴²L. G. Trabuco, E. Villa, E. Schreiner, C. B. Harrison *et al.*, "Molecular dynamics flexible fitting: A practical guide to combine cryo-electron microscopy and X-ray crystallography," Methods 49, 174–180 (2009).
- ⁴³G. Bussi, D. Donadio, and M. Parrinello, "Canonical sampling through velocity rescaling," J. Chem. Phys. 126, 014101 (2007).
- ⁴⁴J. C. Phillips, R. Braun, W. Wang, J. Gumbart *et al.*, "Scalable molecular dynamics with NAMD," J. Comput. Chem. 26, 1781–1802 (2005).
- ⁴⁵ J. Huang, S. Rauscher, G. Nawrocki, T. Ran *et al.*, "CHARMM36m: An improved force field for folded and intrinsically disordered proteins," Nat. Methods 14, 71–73 (2017).
- ⁴⁶J. Perilla and K. Schulten, "Physical properties of the HIV-1 capsid from allatom molecular dynamics simulations," Nat. Commun. 8, 15959 (2017).
- ⁴⁷A. Bakan, L. M. Meireles, and I. Bahar, "ProDy: Protein dynamics inferred from theory and experiments," Bioinformatics **27**, 1575–1577 (2011).
- ⁴⁸N. A. Baker, D. Sept, S. Joseph, M. J. Holst *et al.*, "Electrostatics of nanosystems: Application to microtubules and the ribosome," Proc. Natl. Acad. Sci. U. S. A. **98**, 10037–10041 (2001).
- ⁴⁹T. J. Dolinsky, J. E. Nielsen, J. A. McCammon, and N. A. Baker, "PDB2PQR: An automated pipeline for the setup of Poisson–Boltzmann electrostatics calculations," Nucleic Acids Res. 32, W665–W667 (2004).
- ⁵⁰R. N. Kirchdoerfer, E. O. Saphire, and A. B. Ward, "Cryo-EM structure of the Ebola virus nucleoprotein–RNA complex," Acta Crystallogr., Sect. F: Struct. Biol. Commun. 75, 340–347 (2019).
- ⁵¹ R. N. Kirchdoerfer, D. M. Abelson, S. Li, M. R. Wood *et al.*, "Assembly of the Ebola virus nucleoprotein from a chaperoned VP35 complex," Cell. Rep. **12**, 140–149 (2015).
- ⁵²D. W. Leung, D. Borek, P. Luthra, J. M. Binning *et al.*, "An intrinsically disordered peptide from Ebola virus VP35 controls viral RNA synthesis by modulating nucleoprotein-RNA interactions," Cell. Rep. 11, 376–389 (2015).
- ⁵³U. C. Chaturvedi and R. Shrivastava, "Interaction of viral proteins with metal ions: Role in maintaining the structure and functions of viruses," FEMS Immunol. Med. Microbiol. 43, 105–114 (2005).
- ⁵⁴I. Bahar, T. R. Lezon, L.-W. Yang, and E. Eyal, "Global dynamics of proteins: Bridging between structure and function," Annu. Rev. Biophys. **39**, 23–42 (2010).
- ⁵⁵O. F. Lange and H. Grubmüller, "Can principal components yield a dimension reduced description of protein dynamics on long time scales?" J. Phys. Chem. B 110, 22842–22852 (2006).
- ⁵⁶C. C. David and D. J. Jacobs, "Principal component analysis: A method for determining the essential dynamics of proteins," *Protein Dynamics* (Springer, 2014), pp. 193–226.
- ⁵⁷R. N. Kirchdoerfer, C. L. Moyer, D. M. Abelson, and E. O. Saphire, "The Ebola virus VP30-NP interaction is a regulator of viral RNA synthesis," PLoS Pathog. 12, e1005937 (2016).
- ⁵⁸L. Banadyga, T. Hoenen, X. Ambroggio, E. Dunham, A. Groseth, and H. Ebihara, "Ebola virus VP24 interacts with NP to facilitate nucleocapsid assembly and genome packaging," Sci. Rep. 7, 7698 (2017).